

International Journal of Modern Physics B  
 © World Scientific Publishing Company

## Orbital current signature using neutron diffraction

Dalila Bounoua\*

*Laboratoire Léon-Brillouin, UMR12 CEA-CNRS, Université Paris-Saclay, Gif-sur-Yvette  
 CEDEX, F-91191 France*

William Liège

*Laboratoire Léon-Brillouin, UMR12 CEA-CNRS, Université Paris-Saclay, Gif-sur-Yvette  
 CEDEX, F-91191 France*

Yvan Sidis

*Laboratoire Léon-Brillouin, UMR12 CEA-CNRS, Université Paris-Saclay, Gif-sur-Yvette  
 CEDEX, F-91191 France  
 Institut Jean Lamour, Université Nancy-Artem, Nancy Cedex F- 54011, France*

Philippe Bourges†

*Laboratoire Léon-Brillouin, UMR12 CEA-CNRS, Université Paris-Saclay, Gif-sur-Yvette  
 CEDEX, F-91191 France*

We review the hallmarks of orbital loop currents in various correlated electron materials and how they have been evidenced using polarized neutron diffraction. Over the last 20 years, loop current signatures have been observed in high temperature copper oxide superconductors, iridates, copper oxides spin ladders and recently kagome vanadate superconductors. Such currents induce orbital magnetic moments within the unit cell of these quantum materials that can be detected through their interaction with the neutron spin. In addition to the usual description of orbital moments using point-like local magnetic moments, we here show an alternative description of the neutron magnetic cross-section involving the microscopic currents running between different atomic orbitals. We discuss the corresponding magnetic structure factors and the resulting quantitative differences between both approaches.

*Keywords:* Loop currents; Orbital magnetism; Neutron diffraction.

### 1. Introduction

Orbital loop currents have been one recent noticeable development to describe novel ground states and phenomena in condensed matter. They have been first discussed in the context of high temperature copper oxide superconductors<sup>1,2,3,4</sup> where loop currents occur in the prominent but still mysterious pseudogap phase of these materials. Using polarized neutron diffraction, our team played a major role in the

---

\*dalila.bounoua@cea.fr

†philippe.bourges@cea.fr

2 *D. Bounoua, W. Liège, Y. Sidis & Ph. Bourges*

rising achievement that the loop currents concept is unavoidable for cuprates<sup>5</sup> and recent developments<sup>7,8</sup> may represent the missing link to understand the pseudogap physics.

More recently, their occurrence has also been discussed in a wider range of quantum materials from both experimental and theoretical point of views. However, one major limitation for the establishment of the loop currents concept in quantum matter is that their experimental observations are usually elusive or hidden, and therefore are regularly challenged resulting in alternative theoretical approaches being more widely considered. This has certainly hindered the broader development of the loop-current concept.

The orbital loop currents phenomenon is an example of multipolar order in quantum materials. In cuprates, it is associated with a toroidal moment or anapole polar vector, which appears at the same order as quadrupoles in the expansion of the magnetic energy<sup>6</sup>. In general, loop current would occur in materials with strong interplay between topology, unconventional superconductivity and strong electron–electron correlations, and a wide range of materials could fall into this category.

Indeed, in addition to high- $T_c$  cuprates where they may play a significant role for the pseudogap physics, the existence of orbital loop currents seems ubiquitous in a wide range of quantum materials. In particular, similar type of orbital loop currents phases have been reported using polarized neutron diffraction in iridates<sup>9</sup>, spin-ladder materials<sup>10</sup> and kagome superconductors<sup>11</sup>. These phases are also proposed to be at the origin of the emergence of anomalous physical properties in quantum materials. This is the case of recent reports suggesting that these phases can be relevant for various transport properties, including anomalous Hall effect for instance, in materials consisting of transition metal–doped  $(\text{Bi,Sb})_2\text{Te}_3$ <sup>12</sup> or in twisted bilayer graphene aligned to hexagonal boron nitride<sup>13</sup>. In ferrimagnetic  $\text{Mn}_3\text{Si}_2\text{Te}_6$ , an exotic quantum state is driven by  $ab$  plane chiral orbital currents flowing along edges of  $\text{MnTe}_6$  octahedra<sup>14</sup>. The  $c$  axis orbital moments induced by the in-plane orbital currents couple with the ferrimagnetic Mn spins, drastically enhancing the  $ab$  plane conductivity and yielding colossal magnetoresistance when an external magnetic field is applied along the hard  $c$ -axis. In  $\text{CsV}_3\text{Sb}_5$ , chiral transport was reported in the absence of structural chirality<sup>15</sup>. Remarkably, the transport handedness is found to be switchable by the application of small magnetic fields, and is interpreted as arising from time-reversal symmetry breaking orbital loop currents. Together, these examples highlight the unique magnetoelectric character of loop-current states, in which charge and magnetic degrees of freedom are intrinsically intertwined within a single order parameter, underscoring the broader relevance of the loop-current paradigm for understanding and controlling emergent physical properties in quantum materials such as colossal magnetoresistance or chiral transport.

In this short review, we will first describe the neutron diffraction results in cuprates where the loop current signatures are the most documented. Next, we will

describe how to reformulate the neutron cross-sections for such a complex magnetic object, going beyond the simple point-like moment induced by closed loop currents. Finally, we will review neutron diffraction results indicating loop currents in other strongly correlated materials.

## 2. Copper oxide superconductors

Superconducting cuprate materials are remarkable not only because of their high superconducting critical temperature, but also owing to the occurrence of a mysterious state of matter, the pseudogap (PG) phase, out of which superconductivity emerges<sup>16</sup>. Below its onset temperature  $T^*$ , this state is characterized by the disappearance of large portions of the Fermi surface, which reduces to Fermi arcs<sup>17</sup>. The thermodynamic signature of a phase transition to the pseudogap was first pointed out using high precision magnetization measurements in  $\text{YBa}_2\text{Cu}_3\text{O}_{6+x}$  (YBCO)<sup>18</sup>. Later, resonant ultra-sound (Rus)<sup>19</sup> and subsequently torque measurements<sup>20,21</sup>, provided compelling evidence that the pseudogap phase was a true symmetry breaking state. However, the nature of the order parameter and the broken symmetry remain elusive. There are several experimental evidences showing that discrete symmetries are broken at  $T^*$ , such as the inversion (or parity P) symmetry as reported by optical second harmonic generation (SHG)<sup>22</sup>, the time reversal (T) symmetry through multiple polarized neutron diffraction experiments<sup>5</sup>, Kerr effect<sup>23</sup>, muon spin spectroscopy ( $\mu\text{Sr}$ )<sup>24,25</sup>, as well as the fourfold (rotational R) symmetry deduced from torque measurements<sup>20,21</sup>. Fig. 1 shows the actual phase diagram versus hole doping for two cuprate families, YBCO and  $\text{HgBa}_2\text{CuO}_{4+\delta}$  (Hg1201), gathering data points from various techniques reporting a broken symmetry at  $T^*$ . The pseudogap decreases with increasing doping across the cuprates phase diagram (Fig. 1). It is usually depicted by a linear behaviour although it can depart from that as it is suggested here in YBCO. The discussed broken symmetries occur exclusively in the mysterious pseudo-gap phase and can be readily understood by the existence of orbital loop currents as we shall discuss in this review.

### 2.1. $\mathbf{q} = 0$ *intra-unit-cell order*

Among the above-mentioned experimental evidences of discrete symmetry breaking in the pseudogap state, polarized neutron diffraction technique played a major role to reveal the existence of a magnetic order, defines as a  $\mathbf{q} = 0$  intra-unit-cell (IUC) order. The  $\mathbf{q} = 0$  polarized neutron diffraction results have been recently reviewed in ref <sup>5</sup>. The observed IUC magnetism is reported in the latest experimental phase diagrams (Fig. 1) and suggests that the IUC order is bound to the pseudogap state, preserving the lattice translational symmetry invariance ( $\mathbf{q} = 0$ ), but breaking discrete Ising-like symmetries: time reversal (T), parity (P) and the fourfold rotation (R) symmetries. This has been established in three different cuprates families: YBCO<sup>26,27</sup>, Hg1201<sup>28</sup> and  $\text{Bi}_2\text{Sr}_2\text{CaCu}_2\text{O}_{8+\delta}$ <sup>29</sup>. In a fourth cuprate material,  $\text{La}_{1.9}\text{Sr}_{0.1}\text{CuO}_4$ , the magnetic signal is found at short range and at lower

4 *D. Bounoua, W. Liège, Y. Sidis & Ph. Bourges*

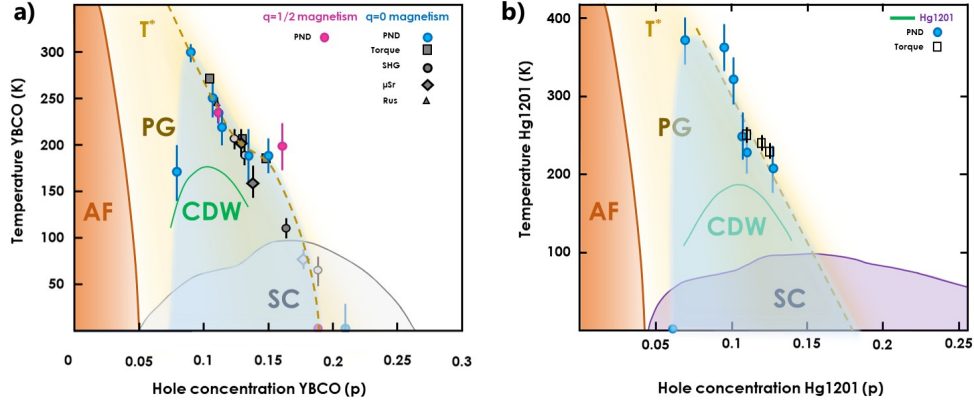


Fig. 1: **High- $T_C$  superconducting (SC) cuprates phase diagram** versus hole concentration showing broken symmetries at the pseudogap (PG) temperature,  $T^*$ , that can be accounted for by loop currents: (a) for  $\text{YBa}_2\text{Cu}_3\text{O}_{6+x}$  (YBCO) bilayer system and (b) for the single layer material  $\text{HgBa}_2\text{CuO}_{4+\delta}$  (Hg1201). The figures are adapted from<sup>5</sup> where the  $\mathbf{q} = 0$  intra unit cell (IUC) magnetism was reviewed along with other techniques which reported broken symmetries at  $T^*$  (see text). AF and CDW refer to antiferromagnetism and charge density wave, respectively. Data for the  $\mathbf{q} = 1/2$  magnetism in YBCO are included from<sup>7,8</sup>. Absence of  $\mathbf{q} = 0$  IUC magnetism at low doping in Hg1201 has been recently reported<sup>34</sup>.

temperature<sup>30</sup>. The intra-unit-cell order has been as well visualized at low temperature in  $\text{Bi}_2\text{Sr}_2\text{CaCu}_2\text{O}_{8+\delta}$  copper oxides using Fourier transform analysis of spectroscopic imaging scanning tunneling microscopy<sup>31</sup>. In that later case, the IUC order is detected through the breaking of the R symmetry.

Remarkably, in these different cuprates, the IUC magnetism shows up concomitantly with the PG state previously established through many different physical properties<sup>16</sup>. For instance, in YBCO, it maps the slight downturn in temperature of the resistivity<sup>32</sup> associated with the pseudogap onset. The polarized neutron diffraction data allow defining a temperature  $T_{mag}$ <sup>26</sup> for the onset of the  $\mathbf{q} = 0$  IUC magnetic signal, which matches, in a large hole-doping range  $p = [0.08-0.2]$  the pseudogap temperature,  $T^*$ . However, at lower doping, the  $\mathbf{q} = 0$  magnetism vanishes in both YBCO<sup>33</sup> and Hg1201<sup>34</sup> and does not follow the expected doping dependence of the pseudogap, possibly due to the proximity of the long range antiferromagnetic phase associated with copper spins. Clearly, the observed broken symmetries and the  $\mathbf{q} = 0$  IUC signatures correspond to what can be expected from an orbital loop current state<sup>1,2,3,4,5</sup>. For instance, a clear magnetic moment is observed along the c axis perpendicular to the  $\text{CuO}_2$  plaquette, even if a noticeable in-plane magnetic component is also detected (see<sup>5</sup> for different possible explanations).

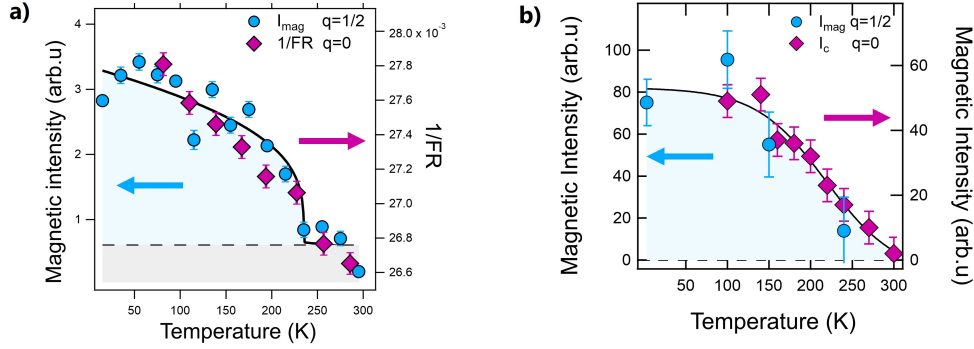


Fig. 2: **Temperature dependence:** (a) Comparison of the temperature dependence in the same  $\text{YBCO}_{6.6}$  sample of the total magnetic signal at  $(0.5,0,0)$  ( $\mathbf{q} = 1/2$ ) as extracted from XYZ polarization analysis (XYZ-PA) (from<sup>7</sup>) and the  $\mathbf{q} = 0$  IUC magnetic order measured at the  $(1,0,0)$  Bragg peak and represented by the inverse of the flipping ratio  $1/FR$  (from<sup>36</sup>). (b) Comparison of the temperature dependence in  $\text{YBCO}_{6.9}$  of the total magnetic signal at  $(0.5,0,0)$  ( $\mathbf{q} = 1/2$ ) as extracted from XYZ-PA (from<sup>8</sup>) and the one of the intra unit cell magnetic order ( $\mathbf{q} = 0$ ) measured at the  $(1,0,0.25)$   $\mathbf{Q}$ -position measured for a similar doping (from<sup>37</sup>).

In the bilayer system  $\text{YBa}_2\text{Cu}_3\text{O}_{6.6}$ , a strong  $a/b$  anisotropy of the intra-unit-cell magnetic structure factor is further observed in detwinned samples<sup>36</sup>, in addition with a particular  $L$  dependence of the structure factor. As a consequence, the correlation of loop currents between the 2 adjacent  $\text{CuO}_2$  plane is actually neither in phase nor out-of-phase, but instead one observes a crisscrossed arrangement of loop currents in the bilayers<sup>36</sup>. In terms of anapoles, that could be interpreted as an averaged bilayer toroidal axis always pointing along a given direction, the orthorhombic  $\mathbf{b}$  direction.

## 2.2. Second type of magnetic ordering

More recently, a second type of magnetic signal has been detected in the pseudogap state of  $\text{YBCO}$ <sup>7,8</sup>. This signal was again observed using polarized neutron diffraction, for several hole-doping levels in the same  $\text{YBCO}$  samples (see Fig. 1.a). This second type of magnetism has been detected with a planar propagation wave vector  $(1/2,0)$  and/or  $(0,1/2)$ , defining a  $\mathbf{q} = 1/2$  magnetic signal. While the  $\mathbf{q} = 0$  magnetism is at rather long range in the limit of the experimental conditions with 3D magnetic correlation lengths typically larger than  $\gtrsim 100 \text{ \AA}$ <sup>27,35</sup>, the  $\mathbf{q} = 1/2$  magnetism is at shorter range: its correlation length has been measured to be about 6-8  $\text{CuO}_2$  unit cells, more precisely  $\xi_{a,b} = 24 \pm 4 \text{ \AA}$  in  $\text{YBCO}_{6.6}$ <sup>7</sup> and  $\xi_{a,b} = 30 \pm 3 \text{ \AA}$  in  $\text{YBCO}_{6.9}$ <sup>8</sup>. These results suggest short range biaxial magnetic correlations corresponding to a quadrupling ( $2 \times 2$ ) of the unit cell.

6 *D. Bounoua, W. Liège, Y. Sidis & Ph. Bourges*

As shown by Fig. 2, the  $\mathbf{q} = 1/2$  magnetism onset temperature exhibits the same doping dependence as the  $\mathbf{q} = 0$  signal. This is striking as it was independently measured on different neutron instruments and happens for two different doping levels, namely, in the underdoped and optimally doped regimes, covering a wide range of doping, while it vanishes beyond the pseudogap state, in the slightly overdoped region. As we shall see below, both types of magnetism are related and found to co-exist in the same temperature and doping ranges as reported in the YBCO phase diagram (Fig. 1.a). The magnetic moment direction has been determined using longitudinal XYZ-polarisation analysis (XYZ-PA) that allows to measure the different magnetic components. The largest magnetic component at  $\mathbf{q} = 1/2$  is clearly  $I_c$  associated with the scattered intensity along the  $c$ -axis, perpendicular to the  $\text{CuO}_2$  plane. Interestingly, XYZ-PA established that only that magnetic component,  $I_c$ , vanishes at  $T^*$ , whereas, in contrast, the much weaker in-plane magnetic component does not change across  $T^*$ . At higher doping, similar temperature dependencies of  $I_c$  magnetic signals at both wave-vectors have been also reported<sup>8</sup> (Fig. 2.b), underlying the close relation between both phenomena. However, at both dopings, the magnetic amplitude of the  $\mathbf{q} = 1/2$  signal is much weaker (about 10-15 times) than the  $\mathbf{q} = 0$  component. The short range  $\mathbf{q} = 1/2$  magnetism then corresponds to a small volume fraction co-existing with larger  $\mathbf{q} = 0$  domains. Interestingly, both types of magnetism exhibit the same magnetic form factor (grey line Fig. 3.a-b) which does not correspond to what would be expected from Cu or even from oxygen spins<sup>8,29</sup> but strongly suggesting a common origin. Finally, let us remark that this second magnetic response at  $\mathbf{q} = 1/2$  has been so far only observed in YBCO. Other cuprates are currently under study to search for the  $\mathbf{q} = 1/2$  magnetic signal.

### 2.3. Not Cu spin moments

We now discuss how to interpret both types of magnetism reported so far. First, let us remind that strong antiferromagnetic (AF) spin correlations are present in copper oxide superconductors in most part of their phase diagram. At low doping, the cuprates phase diagram is characterized by long range antiferromagnetism associated with copper spins<sup>16</sup>. At higher doping, spin fluctuations have been observed using numerous techniques among which inelastic neutron scattering played an important role (see *e.g.* Sidis *et al.*<sup>38</sup>). For instance, as shown recently in the single-layer Hg1201 material<sup>34</sup>, a strong AF response in both the superconducting and pseudogap states is found around the commensurate wavevector  $\mathbf{q}_{\text{AF}} = (0.5, 0.5)$  over a wide energy and doping range<sup>42</sup>. In the archetypal single-layer cuprate,  $\text{La}(\text{Sr},\text{Ba})\text{CuO}_4$ , low energy magnetic fluctuations are instead found at an incommensurate wavevector shifted from  $\mathbf{q}_{\text{AF}}$  (see *e.g.*<sup>39</sup>). They are typically associated with copper spin-density-wave or charge stripe correlations, which form magnetic AF domains; this has been well documented<sup>40</sup> but does not occur in single-layer Hg1201 materials<sup>34</sup>, which exhibit the undistorted tetragonal prototype structure.

In contrast to the Cu spin low energy fluctuations that remain located at or

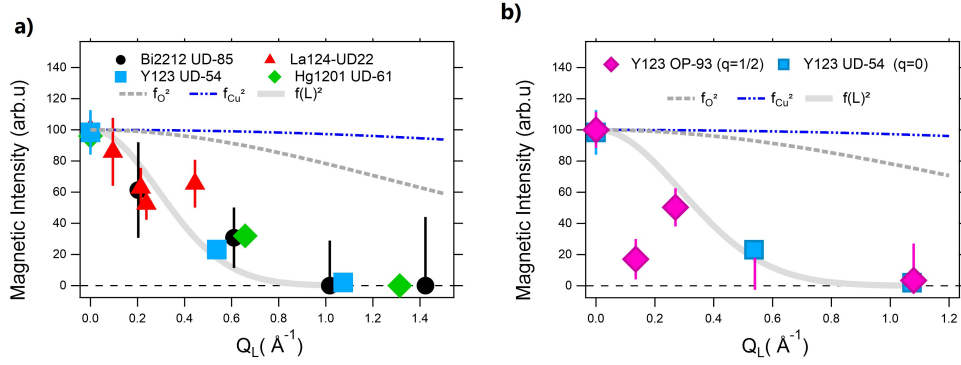


Fig. 3:  **$L$ -dependence:** (a)  $L$ -dependence of the  $\mathbf{q} = 0$  magnetism measured on four cuprate families (from<sup>29</sup>). The plot is made versus the wavevector  $Q_L = \frac{2\pi}{c}L$  in order to compare the four different cuprates. (b)  $L$ -dependence of the  $\mathbf{q} = 1/2$  magnetism measured on two YBCO samples (from<sup>8</sup>). The point at  $Q_L \sim 0.15\text{\AA}^{-1}$  is lower due to extra  $L$  structure factor dependence. The same form factor is obtained for both signals corresponding to the same grey full line.

close to  $\mathbf{q}_{AF}$  with a neutron scattering intensity weighted by the Cu magnetic form factor, the new magnetic responses discussed above are located either close to  $\mathbf{q} = 0$  or  $\mathbf{q} = 1/2$  and are characterized by a very unique form factor. Likewise, in bilayer cuprates, the low energy response of Cu-spin fluctuations correlate in anti-phase within the  $\text{CuO}_2$  bilayer, whereas a criss-crossed loop currents arrangement is instead observed for the  $\mathbf{q} = 0$  IUC order<sup>36</sup>. It is important to stress that neither the  $\mathbf{q} = 0$  nor the  $\mathbf{q} = 1/2$  magnetic responses can be interpreted using copper spins. Indeed, there is a single copper spin per elementary atomic cell in monolayer materials that cannot produce a  $\mathbf{q} = 0$  magnetic response, except in the form of ferromagnetism. This can be ruled out according to macroscopic magnetization measurements. Further, the ordering at  $\mathbf{q} = 1/2$  could be in principle interpreted by spins moments at one site over two Cu-sites with an antiferromagnetic coupling along the unit cell diagonal<sup>7</sup>, but which is not compatible with the known large first neighbour AF superexchange between copper spins in cuprates<sup>41</sup>. It is worth stressing that the relation between the AF spin fluctuations response and the  $\mathbf{q} = 0$  IUC response, which has been experimentally established in two cuprates<sup>42</sup>, did not receive theoretical attention, yet.

#### 2.4. Orbital loop currents

In addition to the observed propagation wavevectors which are not consistent with spin ordering, other experimental features favor interpretation of the data in terms of orbital loop currents. First, a large magnetic moment component is observed to point along the  $c$ -axis perpendicular to the  $\text{CuO}_2$  planes. This is expected for loop

8 *D. Bounoua, W. Liège, Y. Sidis & Ph. Bourges*

currents but is not consistent with spins ordering in cuprates due to their strong XY spin anisotropy<sup>45</sup>. Second, the observed magnetic form factor along  $c^*$  is unusual with a rapid drop at large  $L$  values<sup>8,29</sup> (Fig. 3), which is inconsistent with the ones expected for spins. Instead, it can support orbital magnetic moments induced by loop currents with an extended geometry in real space along the  $c$  axis. It should be also stressed that the form factor has to be strongly anisotropic as the fast decay is not observed along the in-plane wavevectors, otherwise no signal would have been detected using polarized neutron diffraction (see next section).

Considering that the  $\mathbf{q} = 0$  and  $\mathbf{q} = 1/2$  magnetic responses bear similarities (same temperature dependence with appearance at  $T^*$ , same form factor, out-of-plane response), one may wonder whether they could share a common origin or not. We proposed a complex magnetic texture<sup>7,8</sup> where both types of magnetic responses occur in a unified picture. The model is based firstly on the orbital loop current state, referred to as  $CC-\Theta_{II}$ <sup>1,2</sup>. The loop current phase was first developed as an order parameter for the pseudogap phase. The proposed  $CC-\Theta_{II}$  state was actually the primary motivation to search for  $\mathbf{q} = 0$  magnetism in cuprates. It corresponds to a coherently circulating phase between copper and oxygen orbitals within the  $CuO_2$  planes, yielding two opposite orbital magnetic moments perpendicular to it that can be probed with neutron diffraction. The  $CC-\Theta_{II}$  state with  $mmm$  symmetry<sup>1</sup> is represented in Fig. 4.a with its fourfold degenerate ground states. It can be equivalently described by a polar anapole vector either located at the copper site (as in Fig. 4.a) or at the center of the unit cell<sup>5</sup>. The four degenerate ground states correspond to a  $\pi/2$  rotation of the anapole vector.

For each of the degenerate ground states, loop currents flowing among copper and oxygen orbitals form a "butterfly"-shape, which represents the building block of each unit cell. These basic units can correlate in different ways from one unit cell to another leading to different types of orbital magnetic phases. Some examples relevant for interpreting the neutron experiments are shown in (Fig. 4.b-d), where only the anapole vector is represented in each unit cell. In case of a uniform distribution of the anapole vectors (Fig. 4.b), it gives a  $\mathbf{q} = 0$  magnetic order (ferro-anapolar order) with a magnetic intensity maximum at  $\mathbf{Q}=(1,0,0)$  or  $(0,1,0)$  Bragg peaks as it was experimentally observed<sup>5,26,35</sup>. As the four ground states are degenerate, four types of domains are possible and contribute to the magnetic Bragg scatterings.

Interestingly, in case of a coherent correlation between the four domains (as shown in (Fig. 4.c), the resulting pattern establishes a new period for the magnetic structure related to the size of the large domains containing  $P \times P$  unit cells ( $P=20$  in Fig. 4.b-d). It yields loop currents super-cells, characterized in momentum space by a set of satellites magnetic peaks located at  $\delta = \pm \frac{1}{2P}$  from the nuclear Bragg reflections. This occurrence was first theoretically proposed by Varma<sup>43</sup> to account for the Fermi arcs observed in the pseudogap state of cuprates<sup>17</sup>. Broken inversion and chiral symmetries were next experimentally reported using circular and linear photogalvanic responses<sup>44</sup> with a deduced chiral and parity-breaking  $mm2$  symmetry<sup>44</sup> in agreement with the proposed pattern<sup>43</sup> (Fig. 4.c). However, that

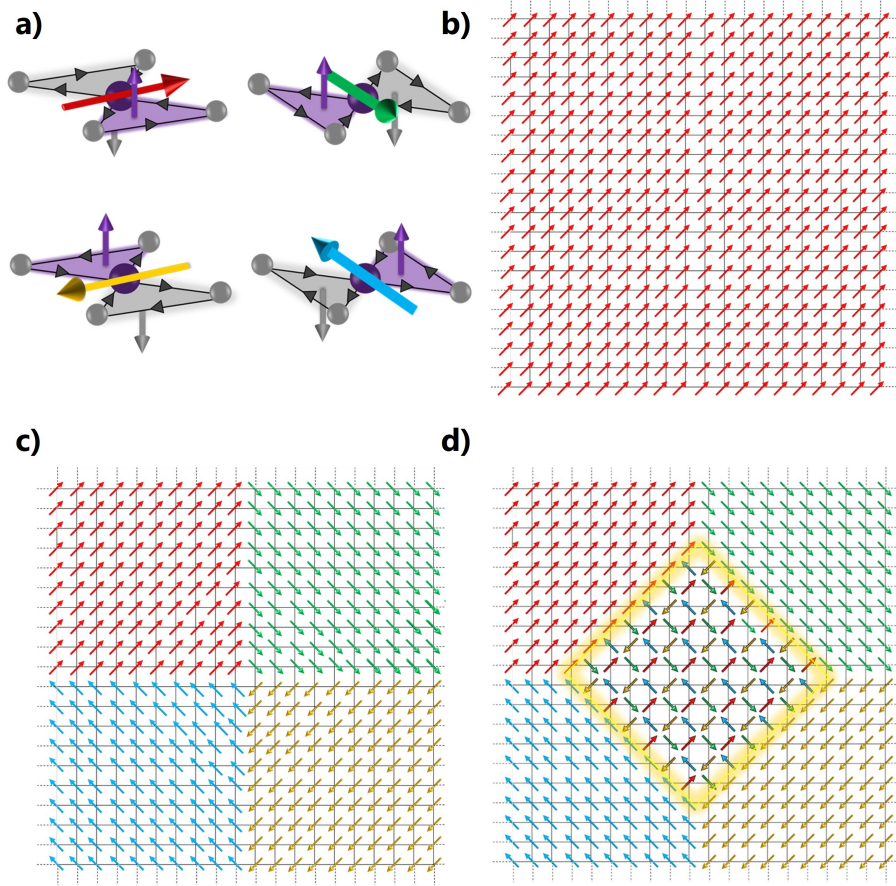


Fig. 4: **Orbital loop currents phases:** (a) Four different degenerated loop currents states. Each spontaneous circulating currents (black arrows) comprises two loops circulating clockwise (in gray) and anti-clockwise (in purple) leading to two magnetic moments along the  $c$  axis perpendicular to the  $\text{CuO}_2$  planes. The 4 possible patterns are characterized by horizontal colored arrows, corresponding to 4 distinct anapole polar vectors centered at the Cu-site. (b) Uniform pattern of one anapole state with  $20 \times 20$   $\text{CuO}_2$  unit cells, (c) Anapole vortex pattern of the 4 anapoles as proposed by Varma<sup>43</sup> and (d) 2D magnetic texture with  $20 \times 20$  unit cells paved by the 4 anapoles. The central cluster reproduces the  $\mathbf{q} = 1/2$  magnetism with  $2 \times 2$  loop current patterns binding large ferro-anapolar domains corresponding to the  $\mathbf{q} = 0$  magnetism (from<sup>7,8</sup>).

pattern has not yet been confirmed using diffraction techniques, most likely because the expected ordering incommensurate wavevector is very small. So that, the magnetic satellites remain hidden by the instrumental neutron resolution function

10 *D. Bounoua, W. Liège, Y. Sidis & Ph. Bourges*

in the nuclear Bragg peak shoulders<sup>8</sup>. Other diffraction techniques such as resonant X-ray scattering should be employed to observe such satellites although one needs first to establish what would be the signature of loop currents in resonant X-ray experiments.

Following these considerations, we realized that a loop current model with the smallest possible domain size  $P=1^{5,7}$ , that can be described as an anapole vortex, can account for the  $2\times 2$  larger unit cells related to the  $\mathbf{q} = 1/2$  ordering. We then developed a complex magnetic texture, represented in Fig. 4.d, to account for both long range  $\mathbf{q} = 0$  magnetic ordering and the short range  $\mathbf{q} = 1/2$  correlations<sup>7,8</sup>. That texture mixes smaller regions in the  $\text{CuO}_2$  plane having loop currents that break the lattice translational symmetry with larger regions in the  $\text{CuO}_2$  plane that respect the translation symmetry. The size of the  $2\times 2$  anapole vortex over the total size of the pattern determines the ratio of intensities between both features assuming that the local orbital magnetic moment amplitude is the same at every site. That complex loop current texture is able to produce a magnetic pattern combining broad scatterings at  $\mathbf{q} = 1/2$  and sharper satellites so close to Bragg reflections  $(1,0)/(0,1)$  that they cannot be resolved experimentally<sup>8</sup>. This texture of uniform and vortex anapoles offers then a nice description of the neutron structure factor in momentum space.

### 3. Polarized neutron cross sections

The multiple results in cuprates suggest that a loop current state could be a generic feature of their phase diagrams. To learn more about their nature, it is important to be as quantitative as possible. It is then interesting to discuss the neutron scattering cross section associated with loop currents, which is a rather unusual object. In particular, as the building block is the "butterfly"-pattern, one needs to calculate the structure factor associated to each of the individual patterns shown in Fig. 4.a.

In case of elastic magnetic scattering, the neutron intensity is proportional to the square of the magnetic structure factor  $|F_M(\mathbf{Q})|^2$ . The magnetic neutron cross section can then be written as<sup>46</sup>,

$$\left. \frac{d\sigma}{d\Omega} \right|_{mag} = \sum_{\tau} |F_M(\mathbf{Q})|^2 \delta(\mathbf{Q} - \tau) \quad (1)$$

$F_M(\mathbf{Q})$  is the magnetic structure factor at the momentum transfer  $\mathbf{Q}$ .  $\tau$  represents the propagation wavevector of the loop current state where the magnetic signal is expected in momentum space depending on the correlations between individual "butterflies". Following our discussion above,  $\tau$  corresponds to the Bragg reflections of the lattice for  $\mathbf{q} = 0$  or the Brillouin zone boundary for the  $\mathbf{q} = 1/2$  correlations. The  $\delta$ -function in Eq. 1 can be replaced by a Gaussian or Lorentzian function in case of short range correlations as it is the case for  $\mathbf{q} = 1/2$  magnetism<sup>7,8</sup>.

For a polarized neutron diffraction experiment, the magnetic structure factor reads<sup>46</sup>,

$$F_M(\mathbf{Q}) = \frac{r_0}{2} \langle \pm | \sigma \cdot \mathbf{B}(\mathbf{Q}) | \pm \rangle \quad (2)$$

$\sigma$  are Pauli matrices describing the neutron spin which can take the two states:  $|+\rangle$  and  $|-\rangle$ . They are related to neutron moment as  $\mu_{\mathbf{N}} = -\gamma\mu_N\sigma$  where  $\mu_N$  is the nuclear magneton and  $\gamma=1.913$  is the gyromagnetic ratio. The prefactor  $r_0 = 0.54 \cdot 10^{-12}$  cm corresponds to the neutron magnetic scattering length for a magnetic moment of 1 Bohr magneton ( $\mu_B$ ) ( $r_0/\gamma$  is the classical radius of the electron). Using Eq. 2, one can take advantage of the great strength of polarized neutron diffraction using XYZ-polarization analysis (XYZ-PA)<sup>7,35</sup> to extract the magnetic signal from the background and determine its different components.

The key term in Eq. 2,  $\mathbf{B}(\mathbf{Q})$ , is proportional to the Fourier transform at the wave vector  $\mathbf{Q}$  of the magnetic field distribution in real space,  $\mathbf{B}(\mathbf{r})$ . There are two possible electronic sources of magnetic field in solids which can interact with the neutron spin, either the magnetic field  $\mathbf{B}_{\mathbf{S}}$  associated with unpaired electron spins, or the magnetic field  $\mathbf{B}_{\mathbf{L}}$  related to electron momentum or currents that can generate orbital moments.  $\mathbf{B}(\mathbf{Q})$  is then in general written as a sum of the spin part and the orbital part as<sup>46</sup>:

$$\mathbf{B}(\mathbf{Q}) = \sum_j \exp(-i\mathbf{Q}\cdot\mathbf{r}_j) \left\{ \hat{\mathbf{Q}} \wedge \mathbf{M}_{\mathbf{S}} \wedge \hat{\mathbf{Q}} + i \frac{I}{2\mu_B} \frac{\hat{\mathbf{Q}} \wedge d\mathbf{l}_j}{Q} \right\} \quad (3)$$

where  $\hat{\mathbf{Q}} = \mathbf{Q}/Q$ .  $\mathbf{M}_{\mathbf{S}}$  is the spin moment,  $I$  is current intensity along the current path  $d\mathbf{l}$ . The sum is made over all magnetic sites,  $j$ , within each unit cell. Usually, only the first spin term is considered in neutron experiments. Here, we only discuss the second one as the copper spins do not contribute for both the  $\mathbf{q} = 0$  and  $\mathbf{q} = 1/2$  magnetism.

For the second term, there are two, in principle assumed to be equivalent, ways to express the neutron cross section arising from the loop currents phase. On the one hand (see *e.g.*<sup>7,35</sup>), one considers a point-like orbital moment that is produced by the circulating current similar to the spin term in Eq. 3. On the other hand (see *e.g.*<sup>47</sup>),  $\mathbf{B}(\mathbf{Q})$  can be expressed in terms of the Fourier transform of the current density. We describe below these two methods to calculate the "butterfly" structure factor for the four CC- $\theta_{II}$  states. It should be stressed that all the calculations in the next sections are strictly only valid for the  $\mathbf{q} = 0$  order where a given pattern is repeated over all the unit cells.

For the sake of simplicity in comparing the resulting structure factors, only one CuO<sub>2</sub> layer per unit cell will be considered. However, in bilayer systems, the structure factor contains an additional  $L$ -dependent factor being related to the correlation of loop currents between the two adjacent CuO<sub>2</sub> planes as it has been reported in YBa<sub>2</sub>Cu<sub>3</sub>O<sub>6+x</sub><sup>36</sup> (see above).

### 3.1. Orbital point-like moment picture of the $CC\text{-}\theta_{II}$ phase

First, one considers, for the orbital part in Eq. 3, point-like orbitals moments induced by the loop currents. For the  $CC\text{-}\theta_{II}$  phase, there are two patterns with anapoles along both diagonals:  $\pm(1,1,0)$  ( $\mathcal{P}_a$ ) and  $\pm(1,-1,0)$  ( $\mathcal{P}_b$ ) directions among the four ground states. The contribution of the two other domains ("time-reversal domains") gives the same structure factor as it depends only on the sign of orbital magnetic moment  $\mathbf{M}_c$  pointing along the  $c$ -axis. Both patterns have a different magnetic neutron structure factor. For the pattern  $\mathcal{P}_a$ , one needs to put opposite moments at  $(-x_0, x_0)$  and  $(x_0, -x_0)$  respectively (Fig. 5.a). For the pattern  $\mathcal{P}_b$ , the orbitals opposite moments are located at the coordinates  $\pm(x_0, x_0)$  (Fig. 5.d) along the unit cell diagonals with  $x_0 = 0.146$ , that defines the geometric center of the loop triangle. The calculated magnetic interaction  $\mathbf{B}(\mathbf{q})$  can then be written as,

$$\mathbf{B}(\mathbf{q}) = 2i f(Q) \sin(2\pi x_0(H \pm K))(\hat{\mathbf{Q}} \wedge \mathbf{M}_c \wedge \hat{\mathbf{Q}}) \quad (4)$$

The sign  $-(+)$  stands for each pattern,  $\mathcal{P}_a$  and  $\mathcal{P}_b$  respectively. One needs to associate a magnetic form factor  $f(Q)$  ( $f(0) = 1$ ) to the orbital magnetic moment  $\mathbf{M}_c$  which should be related to the Fourier transform of involved magnetic atomic orbitals. In principle,  $f(Q)$  should be given by the Fourier transform of the moment distribution associated with a single triangle of the  $CC\text{-}\theta_{II}$  phase. However, this quantity is not obvious to define but should, in principle, be a combination of copper and oxygen orbital form factors.

The Fig. 5.b and Fig. 5.e show the magnetic neutron intensity  $|F_M(\mathbf{Q})|^2$  in the  $(H,K)$  plane calculated using the point-like model for both patterns. For a sake of comparison, no form factor is included. First, the intensity is zero for  $H=K=0$  due to compensated moments within each unit cell. Neutron intensity maps are rotated by  $90^\circ$  to each other with the main contribution to the intensity being located along the diagonals. In Fig. 6.a, the averaged intensity of both patterns assuming equally populated domains is represented, the intensity is maximum along  $a^*$  and  $b^*$ <sup>35</sup>. The neutron intensity would decay at large  $Q$  only due the form factor  $|f(Q)|^2$ .

### 3.2. Array of currents of the $CC\text{-}\theta_{II}$ phase

A second method to treat the orbital term in Eq. 3 is to consider the internal magnetic field originating from the circulating currents<sup>47,48,49</sup>. For a single  $\text{CuO}_2$  plane,  $\mathbf{B}(\mathbf{Q})$  can be expressed in terms of the Fourier transform,  $\mathbf{j}(\mathbf{Q})$ , of the current density  $\mathbf{j} = Id\mathbf{l}$  (represented on Fig. 5, for both possible  $CC\text{-}\theta_{II}$  ground states associated with anapoles at  $90^\circ$ ).  $\mathbf{B}(\mathbf{Q})$  entering in Eq. 2 is then

$$\mathbf{B}(\mathbf{Q}) = -i f(Q) \frac{\hat{\mathbf{Q}} \wedge \mathbf{j}(\mathbf{Q})}{Q} \quad (5)$$

To calculate for each domain the magnetic scattering signal in the  $Q = (H, K)$  reciprocal space, we need to determine  $\mathbf{j}(\mathbf{Q})$  for a given geometry of microscopic

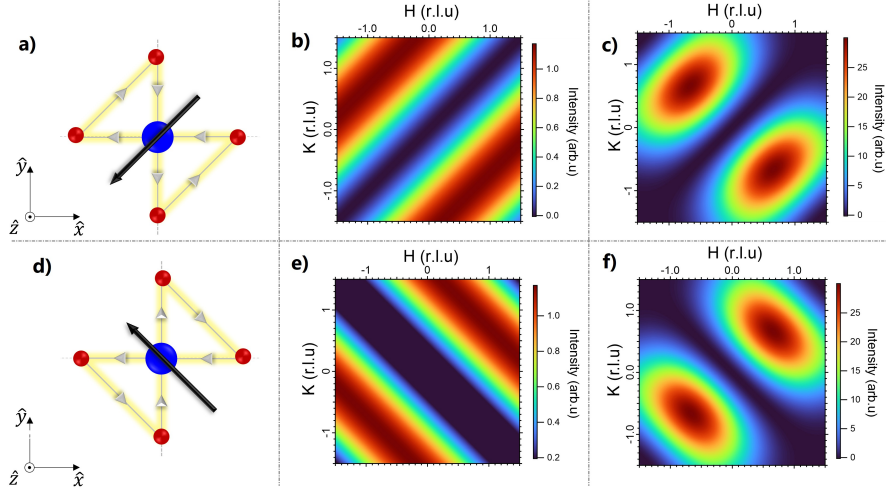


Fig. 5: **Magnetic structure factors:** Magnetic moment distribution for two ground states with (a) the anapole along x+y (pattern  $\mathcal{P}_a$ ) and (d) the anapole along x-y (pattern  $\mathcal{P}_b$ ). Magnetic structure factors calculated for point-like moment located at the center of the loop triangle: (b) for anapole along x+y (pattern  $\mathcal{P}_a$ ) and (e) for anapole along x-y (pattern  $\mathcal{P}_b$ ). Magnetic structure factors calculated from the currents: (c) for the anapole along x+y (pattern  $\mathcal{P}_a$ ) and (f) for the anapole along x-y (pattern  $\mathcal{P}_b$ ). The form factor  $f(Q)$  is not included in the calculations.  $(\hat{x}, \hat{y}, \hat{z})$  defines an orthonormal coordinate system for the tetragonal lattice of cuprates.

wires. First, one defines the current in real space. For instance, for the thread along the  $x$  direction in Fig. 5.a, it gives  $\mathbf{j}_1(\mathbf{r}) = -I\delta(y)\delta(z)\hat{x}$  for  $-a/2 < x < a/2$  where  $I$  is the current flowing in the wires and  $a \simeq 3.85\text{\AA}$  is the lattice parameter. For a "butterfly" current distribution, such as Fig. 5.a, the total current distribution  $\mathbf{j}(\mathbf{r}) = \sum_i \mathbf{j}_i(\mathbf{r})$  is the sum of currents along the different threads forming both triangles. One needs next to perform the Fourier transform of the current distribution. For instance, for the  $j_1$  example above, it yields  $\mathbf{j}_1(\mathbf{Q}) = -Ia \frac{\sin(\pi H)}{\pi H} \hat{x}$ . The Fourier transform of the current distribution,  $\mathbf{j}_a(\mathbf{Q})$  and  $\mathbf{j}_b(\mathbf{Q})$ , for both "butterfly" patterns of Fig. 5, reads

$$\begin{aligned} \mathbf{j}_a(\mathbf{Q}) &= -Ia \frac{\sin(\pi H)}{\pi H} \hat{x} - Ia \frac{\sin(\pi K)}{\pi K} \hat{y} + Ia \frac{\sin(\pi(H+K)/2)}{\pi(H+K)/2} \cos(\pi(H-K)/2) (\hat{x} + \hat{y}) \\ \mathbf{j}_b(\mathbf{Q}) &= -Ia \frac{\sin(\pi H)}{\pi H} \hat{x} + Ia \frac{\sin(\pi K)}{\pi K} \hat{y} + Ia \frac{\sin(\pi(H-K)/2)}{\pi(H-K)/2} \cos(\pi(H+K)/2) (\hat{x} - \hat{y}) \end{aligned} \quad (6)$$

The neutron structure factor Eq. 2 can be deduced using Eqs. 6 in Eq. 5. In this version of the loop current model, the wires are assumed to be infinitely thin. The Fig. 5.c and Fig. 5.f show the magnetic neutron intensity  $|F_M(\mathbf{Q})|^2$  in the (H,K) plane calculated using the currents model for both patterns. Similarities with the

point-like model are clear with a minimum along one diagonal and zero intensity for  $H=K=0$ . However, in contrast with the point-like model, the neutron intensity decays at large  $Q$ , even in the absence of the form factor, due to the  $1/Q$  factor in Eq. 5. The averaged intensity of both patterns assuming that they have the same population for both types of domains is represented in Fig. 6.b. Being more isotropic, the obtained intensity differs noticeably from the one calculated with the point-like moment model shown in Fig. 6.a.

In principle, one needs to add an effective "transverse" thickness,  $\delta$ , of each wire, to account for the typical size of copper and oxygen  $d$  and  $p$  orbitals. This leads to an additional (still empirical) form factor  $f(Q)$  with  $f(0)=1$ , which is similar to the magnetic form factor for point-like moments. It is interesting to notice that the two "transverse" current thicknesses are decoupled from each other and can take distinct values unlike atomic orbitals for point-like moment. Therefore, the related form factor can be in principle anisotropic between in-plane and out-of-plane directions. It is worth to remind that this anisotropy is actually observed experimentally<sup>8,29</sup> (see Fig. 3) although the exact explanation is not yet established.

Basically, in comparison to spin moments, it is usually considered<sup>47,49</sup> that the neutron scattering intensities qualitatively differ for orbital currents due to the characteristic size of the current loop which can be as large as the unit cell distance between the copper atoms,  $a=3.85\text{\AA}$ , whereas it is the size of the copper orbitals,  $a_0 \sim 1.2\text{\AA}$ , for spins. Therefore, it is generally assumed that the neutron intensity from orbital currents is likely to fall off more rapidly with increasing  $Q$  than the usual atomic form factor for a spin moment, that was particularly the case for  $D$ -density wave model<sup>48,49</sup>. The effect can be so important that the expected intensity is often considered to be too small to be detected in neutron experiments. The decreasing intensity is indeed observed for currents in Fig. 5. However, because the discussed loop triangle of the  $CC-\theta_{II}$  phase corresponds to only  $1/8$  of the unit cell area. The expected intensity is actually still sizable in cuprates to be measured in neutron diffraction experiments.

### 3.3. Comparison of neutron intensity obtained with both methods

To be more concrete and compare quantitatively the structure factor obtained via both methods, we expand the relations (Eqs. 4 and 6) for a scattering plane defined by the two reciprocal directions  $(\mathbf{a}^*, \mathbf{c}^*)$ , then  $\mathbf{Q} = 2\pi H/a\hat{\mathbf{x}} + 2\pi L/c\hat{\mathbf{z}}$ . This reciprocal plane  $(H, 0, L)$  was often used as the scattering plane in neutron diffraction experiments.

For the point-like moment model (section 3.1), one obtains a moment perpendicular to the scattering plane,  $\mathbf{M} = M_c\hat{\mathbf{z}}$ . In principle,  $M_c = I\delta^2$  where  $I$  is the current density in the wire defined above and  $\delta^2 = a^2/8$  the cross-section area of each triangle. Then,  $\hat{\mathbf{Q}} \wedge \mathbf{M} \wedge \hat{\mathbf{Q}}$  entering in Eq. 4 becomes  $\frac{M_c H}{H^2 + (a/c)^2 L^2} (-\frac{a}{c} L\hat{\mathbf{x}} + H\hat{\mathbf{z}})$ . Eq. 4 can be rewritten for both domains as,

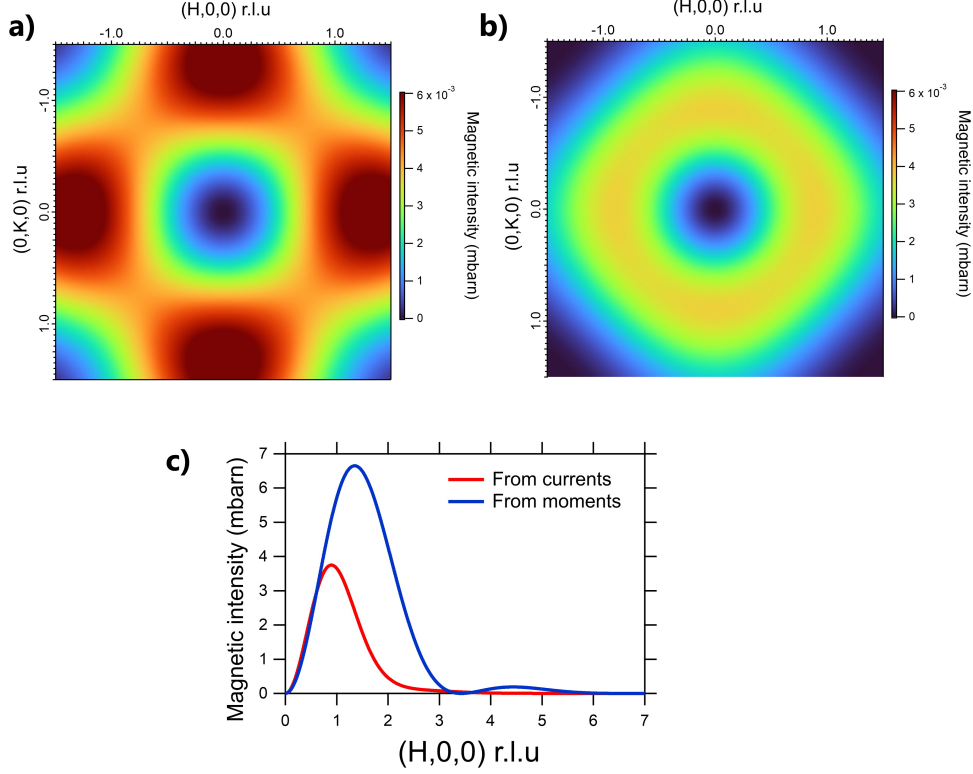


Fig. 6: **Structure factor comparison:** Averaged intensities of both patterns: (a) for the point-like model and (b) for the currents model. (c) Comparison of the structure factors along the H direction for  $K=0$  for both models and assuming the relation  $M_c = Ia^2/8$ . The structure factors are given in mbar for  $M_c = 0.1\mu_B$  as found experimentally<sup>26,35</sup>. In (c), the copper form factor  $|f(Q)|^2$  is also included to compare with neutron diffraction experiments.

$$\mathbf{B}(\mathbf{Q}) = \pm 2if(Q) \sin(2\pi x_0 H) \frac{HM_c}{H^2 + (a/c)^2 L^2} \left[ -\frac{a}{c} L\hat{\mathbf{x}} + H\hat{\mathbf{z}} \right] \quad (7)$$

$c$  is the  $c$ -axis lattice parameter. For the currents model (section 3.2) and  $K = 0$ , the current density for both patterns becomes  $\mathbf{j}_a(\mathbf{Q}) = -\mathbf{j}_b(\mathbf{Q}) = Ia[1 - \frac{\sin(\pi H)}{\pi H}]\hat{\mathbf{y}}$  and  $\mathbf{B}(\mathbf{Q})$  reads

$$\mathbf{B}(\mathbf{Q}) = \pm if(Q) \frac{1}{2\pi} \left(1 - \frac{\sin(\pi H)}{\pi H}\right) \frac{Ia^2}{H^2 + (a/c)^2 L^2} \left[ -\frac{a}{c} L\hat{\mathbf{x}} + H\hat{\mathbf{z}} \right] \quad (8)$$

Interestingly, Eqs. 7 and 8 show clear common similarities about the neutron orientation factor. However, their in-plane dependencies noticeably differ: the Fig.

16 *D. Bounoua, W. Liège, Y. Sidis & Ph. Bourges*

6.c shows along  $H$  and for  $L = 0$  both structure factors  $|\mathbf{B}(\mathbf{Q})|^2$  for a single one "butterfly"-shape loop currents pattern including the form factor  $f(Q)$  for  $\text{Cu}^{2+}$  spins. Clearly, both methods give different results. To compare both models in absolute units, we use the relation  $M_c = Ia^2/8$  between the magnetic flux, the current and the area of one triangle  $a^2/8$ . At  $H=1$ , the intensity ratio of both methods is  $\sim 0.8^2 = 0.64$ . The Fig. 6.c shows the possible correspondence with experiments although there is so far no existing possible comparison as no intra-unit-cell magnetism has been yet detected at larger  $H$ . For instance, at  $\mathbf{Q}=(1,0,0)$ , the expected magnetic intensity in absolute units is found to be  $\sim 5.7$  mbarn from the point-like-moment magnetic structure factor Eq.7 and  $\sim 3.6$  mbarn from the current calculations of the magnetic structure factor Eq. 8. These amplitudes are consistent with the reported IUC magnetic intensity at  $(1,0,0)$  and  $(0,1,0)$  of  $\sim 6$  and  $\sim 2$  mbarn<sup>36</sup> as specified in<sup>7</sup>.

#### 4. Other correlated materials

Loop currents are also discussed as possible instabilities in other quantum materials aside from the superconducting two-dimensional (2D) cuprates. From our perspective, that was not obvious at first as the proposed theory was developed specifically for 2D  $\text{CuO}_2$  layers<sup>1</sup>. However, in recent years, more theoretical approaches for loop currents as well as novel experimental evidences have been made in other materials. We here shall review these novel developments in the following.

##### 4.1. Two-leg ladder cuprates

The first example does not stray too far from 2D cuprates. The two-leg ladder cuprate  $\text{Sr}_{14-x}\text{Ca}_x\text{Cu}_{24}\text{O}_{41}$  hosts a very rich phase diagram with a well-established spin liquid state for a wide range of Ca content. Its crystal structure, called composite, consists in two interacting sub-lattices,  $\text{CuO}$  chains and  $\text{Cu}_2\text{O}_3$  ladders, which are incommensurate along the  $c$  axis.

Using polarized neutron diffraction, we observe novel short range magnetic correlations for two different Ca contents<sup>10</sup>. The magnetic correlations develop exclusively at forbidden Bragg positions of the two-leg ladders sub-lattice. Models involving magnetic moments on Cu or oxygen sites fail to account for the experimental results whereas simple models based on loop currents on the ladders sub-lattice capture the most salient observation of the magnetic scattered intensity<sup>10</sup>. The similarities of the observed phenomena with 2D cuprates are striking. The neutron data show that 50% of the magnetic moment lies out of the ladder planes with a tilt of the moment in agreement with previous estimates in superconducting cuprates<sup>26,36,50</sup>. The short range magnetism remains confined to a single two-leg ladder at low substitution similarly to what has been reported in lightly doped  $(\text{La,Sr})_2\text{CuO}_4$  cuprate where the short-range loop currents correlations are short range, 2D and confined in bond centered charge stripes<sup>30</sup>. Of course, the cause for confinement is different in both systems: in the later case, it is due to the doping and spontaneous stripe

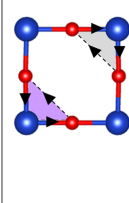
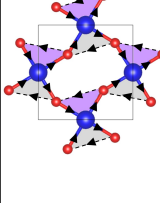
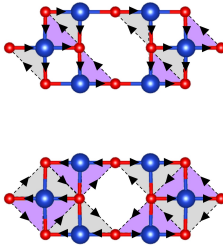
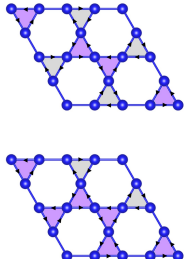
Material family	High Tc cuprates	Iridates	Two-leg ladder cuprates	Kagome superconductors
Dimensionality	2D	2D	Quasi-1D	2D
Loop current pattern				

Fig. 7: **Classification of loop current models:** Different loop current patterns able to reproduce the  $\mathbf{q} = 0$  magnetism in copper oxide superconductors including  $\text{YBa}_2\text{Cu}_3\text{O}_{6+x}$  and  $\text{HgBa}_2\text{Cu}_4\text{O}_{4+x}$ <sup>5</sup>, iridates  $\text{Sr}_2(\text{Ir,Rh})\text{O}_4$ <sup>9</sup> and quasi-1D two leg ladder cuprates  $\text{Sr}_{14-x}\text{Ca}_x\text{Cu}_{24}\text{O}_{41}$ <sup>10</sup>. In the metallic kagome  $\text{CsV}_3\text{Sb}_5$ , two patterns consistent with the neutron diffraction experiments<sup>11</sup> with loop currents on vanadium atoms triangles that respect the CDW symmetry. In the case of two-leg ladder cuprates, the upper model corresponds to the  $CC-\theta_{II}$  phase<sup>1</sup> while the lower pattern corresponds to the model proposed in the context of two-dimensional spin-liquids<sup>3</sup>

formation and in the former case due to the intrinsic structure of the material. The deduced loop current patterns, shown in Fig. 7, adapt themselves to the ladder one quasi-1D atomic structure with increasing inter-ladders correlations with the Ca substitution<sup>10</sup>.

#### 4.2. Iridates

A second example concerns the layered perovskite iridate,  $\text{Sr}_2(\text{Ir,Rh})\text{O}_4$ , which exhibits strong similarities with high-Tc cuprates in terms of layered perovskite structure and electronic states, in spite of a different nature of 5d (iridium) and 3d (copper) orbitals. At low doping, long range antiferromagnetic ordering is present in iridates suggesting complex spin-orbital state represented by an effective total angular momentum,  $J = 1/2$ <sup>51</sup>. These materials also exhibit a PG-like behaviour reminiscent of cuprates in their electronic excitation spectrum<sup>52</sup>. The motivation to search for loop currents in this material was the observation of an hidden order breaking inversion symmetry as reported by optical second harmonic generation (SHG)<sup>53</sup> as it has been subsequently observed in cuprates<sup>22</sup>. Using polarized neutron diffraction, time-reversal broken symmetry was reported concomitantly with the hidden order phase<sup>9</sup> with an onset temperature that matches the odd-parity hidden order

reported by SHG experiments upon Rh substitution<sup>53</sup>. Similarly to loop currents in cuprates the lattice translation invariance was preserved, suggesting that the novel magnetic order and broken symmetries can be explained by the loop-current model, previously predicted for copper oxide superconductors<sup>1</sup>. That result suggests a more generic character of loop currents in correlated electron oxides. The planar structure that involves oxygen ligand could be a key ingredient for the establishment of the loop current phases as shown Fig. 7.

In relation with the AF spin order, there is however an interesting difference between the observation of loop current states in cuprates and iridates that might suggest a different microscopic model for loop current in each material. In iridates, the inversion and time-reversal symmetry breaking are already observed in insulating  $\text{Sr}_2\text{IrO}_4$ , coexisting with the Néel spin order whereas in cuprates the  $\mathbf{q} = 0$  IUC magnetic ordering vanishes at low doping<sup>33,34</sup> (see Fig. 1 above). The existence of the same loop current states in both insulators and metals has been discussed in the presence of a  $Z_2$  topological order<sup>54</sup>. Within this framework, on the square lattice antiferromagnet, loop currents can co-exist with an AF ordered phase with collinear spin correlations as we have reported in iridates. Why it is then not happening in cuprates? This could correspond to two different limits of the same model, which could explain the difference between cuprates and iridates<sup>55</sup>.

### 4.3. *kagome metals*

Another case for loop currents phase recently emerges in metallic kagome materials from their nontrivial band structure. A chiral flux phase has been theoretically predicted in the topological superconductor  $\text{AV}_3\text{Sb}_5$  ( $A = \text{K}, \text{Rb}, \text{Cs}$ ) with a quasi-2D kagome lattice<sup>56,57,58</sup>. These materials exhibit a topological bond or charge density wave (CDW) as described experimentally using X-ray at the  $\mathbf{M}$ -point of the Brillouin zone<sup>59</sup>. In particular, the kagome metal,  $\text{CsV}_3\text{Sb}_5$ , exhibits both a CDW below 94K with the 2x2 doubling of the hexagonal unit cell and a superconducting phase below 2.5K. These materials also show strong anomalous Hall effect<sup>60</sup>, but no spin ordering has been found in these materials both by muon spin spectroscopy and neutron diffraction. Instead, the proposed chiral flux state<sup>56,57,58</sup> breaks time-reversal symmetry yielding anomalous Hall effect as it was long-sought-after by Haldane<sup>61</sup> without relying on spins. Rapidly, time-reversal symmetry breaking were reported in the charge ordered state using muon spin spectroscopy<sup>62</sup>. That was interpreted by loop current states with a current pattern among the triangles of vanadium atoms as shown in Fig. 7 but the exact loop currents pattern can only be deduced from diffraction techniques. Scanning tunnelling microscopy further provides evidence for time-reversal symmetry-breaking in the superconducting state of  $\text{Cs}(\text{V}, \text{Ta})_3\text{Sb}_5$  through the interference between internal magnetism, Bogoliubov quasi-particles and pairing modulation<sup>63</sup>.

We recently perform polarized neutron diffraction on the  $\text{CsV}_3\text{Sb}_5$  material searching for magnetic intensity at momenta positions relative to the CDW<sup>11</sup>. This

measurement was experimentally challenging and went close to the limit in accuracy obtainable with polarised neutron diffraction in a reasonable time. Most models predict loop currents to produce magnetic intensity at the Brillouin zone boundary  $\mathbf{M}$ -points:  $\mathbf{M}_1=(1/2,0,L)$  or  $\mathbf{M}_2=(1/2,1/2,L)$  reciprocal space positions with  $L=0$  or  $1/2$ . We investigated both momenta positions. For the first one, no magnetic signal was observed ruling out the possibility of having a magnetic moment larger than  $0.01 \mu_B$  per vanadium atom. However, measurements at  $\mathbf{M}_2$  suggest the possibility of a magnetic signal, with a tiny magnetic moment of only  $m = 0.02 \pm 0.01 \mu_B$  per vanadium triangle<sup>11</sup>. This shows that current models have to be refined whether toward a lowering of the expected magnetic moment or toward a different loop current pattern giving rise to magnetic intensity at different reciprocal space positions to be compatible with our measurements.

## 5. Conclusions and other developements

Loop currents have emerged over the last decades as a new platform to investigate the interplay between topology, unconventional superconductivity and strong electron–electron correlations. These state corresponds to extended magnetization of the metallic atoms on the ligand atoms through their orbitals hybridization. Orbital loop currents have been suggested either by various novel theoretical predictions or experimental reports showing unexpected symmetry breakings. The former happened in kagome metals where numbered theoretical models encourage experimentalists to push the limit of their experimental techniques. The latter occurred for iridates. Generalization of loop currents phase in other class of quantum materials would certainly grow in the coming years although their identification is usually elusive experimentally.

In cuprates, the observation of loop currents using polarized neutron scattering<sup>5</sup> has given a clear ground for an unforeseen solution for the origin of pseudogap and, as a result, may yield a possible novel scenario for high- $T_c$  superconductivity. Although uniformly ordered flux phases cannot alone be responsible for the pseudogap, topological orders<sup>3</sup>, bond-density wave<sup>4</sup> or pair density wave<sup>72</sup>, to which loop currents are inseparable, would be capable to open a gap at the Fermi surface. Further, even with uniform flux phases, non uniform bond currents can occur<sup>73</sup> and can be responsible for a fermionic gap. A loop current superstructure has been as well proposed to explain the pseudogap<sup>43</sup>. This is so far not observed directly through diffraction techniques.

Experimentally, one instead observes additional short range correlations indicating a complex organisation of anapoles - associated with loop currents - between different unit cells<sup>7,8</sup>. The  $\mathbf{q} = 1/2$  magnetic signal, although very weak, shows a breaking of the translational symmetry with a doubling of the unit cell along both  $a^*$  and  $b^*$  directions that could play an important role for the pseudogap physics together with the  $\mathbf{q} = 0$  magnetism. Aiming at assessing the relationship between the pseudogap phase and both magnetic responses, we are currently extending our

20 *D. Bounoua, W. Liège, Y. Sidis & Ph. Bourges*

study to an underdoped  $\text{YBa}_2\text{Cu}_3\text{O}_{6.4}$  ( $p=0.07$ ) sample closer to the point where spin antiferromagnetic fluctuations become prominent.

Another candidate where to find loop currents is the Fe-based superconducting materials that could also host orbital loop currents<sup>64,65</sup> owing to the spin-orbit coupling present in these compounds, which would enforce the emergence of such an order in addition to the usual stripe-type AF state. The FeSe system is certainly one of the first Fe-based superconductor to look at as there is a nematic state below 90 K and no long-range AF spin order at low temperature.

On a broader view, the loop currents state belongs to the class of multipolar phenomena, a field that has seen an important development in recent years. For instance, the existence of anapoles in a very different system, the ferromagnetic compound  $\text{Sm}_{0.976}\text{Gd}_{0.024}\text{Al}_2$ , was revealed very recently by polarized neutron diffraction<sup>66</sup>. Similarly, an anapolar contribution to the magnetism of Cr-doped  $\text{V}_2\text{O}_3$ <sup>67</sup> was measured using resonant X-ray diffraction. This opens potential new routes for the observation of multipolar physics. More recently, a multipolar order underlying spin magnetism was also predicted in altermagnets<sup>68,69</sup>, for instance in  $\text{MnF}_2$  due to the symmetry of the lattice near the Mn site related to neighboring fluorine atoms. These multipoles are thought to be essential to establish altermagnetism. Experiments are currently underway to determine if the predicted magnetic octupoles are relevant or not in  $\text{MnF}_2$ .

$\text{URu}_2\text{Si}_2$  is another emblematic material with strong electronic correlations and puzzling physical properties, in particular the existence of an enigmatic hidden order below  $\sim 17.5\text{K}$ . Recent theoretical attempts describe its complex physics by related orbital current states<sup>70,71</sup>. A chiral spin liquid has been proposed to account for the hidden order<sup>71</sup>. This state involves different types of loop currents (which do not necessarily break the translation of the lattice). Another approach proposes toroidal quadrupoles, implying a complex magnetic pattern with ferro-vortex and antiferro-vortex moments<sup>70</sup>.

Finally, loop current physics would certainly be of paramount importance in compounds where quantum criticality and quantum fluctuations play a major role. Cuprates, heavy fermions and iron-based superconductors can be considered as promising candidates. Original ideas induced by exchanges between theory and experiment shall generate new perspectives and the design of novel experiments, in order to firmly establish the loop current paradigm in solid-state science.

## Acknowledgements

We wish to thank Vivek Aji and Benoît Fauqué with who we initiated the currents approach for the neutron diffraction structure factor. We acknowledge financial support from the ANR JCJC project NEXUS (Contract ANR-23-CE30-0007-01) of the Agence Nationale de la Recherche (ANR) French agency and the 2FDN - Fédération Française de la Diffusion Neutronique.

**ORCID**

Dalila Bounoua - <https://orcid.org/0000-0003-0860-1321>

W. Liège - <https://orcid.org/0009-0001-9126-2318>

Yvan Sidis - <https://orcid.org/0000-0002-9333-0169>

Philippe Bourges - <https://orcid.org/0000-0001-9494-0789>

**References**

1. C. M. Varma. Theory of the pseudogap state of the cuprates. *Phys. Rev. B*, 73:155113, Apr 2006.
2. C. M. Varma. Colloquium: Linear in temperature resistivity and associated mysteries including high temperature superconductivity. *Rev. Mod. Phys.*, 92:031001, Jul 2020.
3. M. S. Scheurer and S. Sachdev, Orbital currents in insulating and doped antiferromagnets *Phys. Rev. B*, 98:235126, Dec 2018.
4. S. Sarkar, D. Chakraborty and C. Pépin, Incipient loop-current order in the underdoped cuprate superconductors *Phys. Rev. B*, 100:214519, Dec 2019.
5. P. Bourges, D. Bounoua and Y. Sidis, Loop currents in quantum matter *C. R. Physique*, 22;7, 2021
6. S. Di Matteo, and M. R. Norman, Orbital currents, anapoles, and magnetic quadrupoles in CuO *Phys. Rev. B*, 85:235143, Jun 2012.
7. D. Bounoua, Y. Sidis, T. Loew, F. Bourdarot, M. Boehm, P. Steffens, L. Mangin-Thro, V. Balédent and P. Bourges, Hidden Magnetic Texture in the Pseudogap Phase of High-Tc YBa<sub>2</sub>Cu<sub>3</sub>O<sub>6+x</sub> *Comm. Phys.*, 5:268, Nov 2022.
8. D. Bounoua, Y. Sidis, T. Loew, F. Bourdarot, M. Boehm, P. Steffens, L. Mangin-Thro, V. Balédent and P. Bourges, Universality of  $q = 1/2$  orbital magnetism in the pseudogap phase of the high-Tc superconductor YBa<sub>2</sub>Cu<sub>3</sub>O<sub>6+x</sub> *Phys. Rev. B*, 108:214408, Dec 2023.
9. J. Jeong, Y. Sidis, A. Louat, V. Brouet, and P. Bourges, Time-reversal symmetry breaking hidden order in Sr<sub>2</sub>(Ir,Rh)O<sub>4</sub>, *Nat. Comm.*, 8:15119, Apr 2017.
10. D. Bounoua, L. Mangin-Thro, J. Jeong, R. Saint-Martin, L. Pinsard-Gaudart, Y. Sidis, and P. Bourges, Loop currents in two-leg ladder cuprates *Comm. Phys.*, 3:123, Jul 2020.
11. W. Liège, Y. Xie, D. Bounoua, Y. Sidis, F. Bourdarot, Y. Li, Z. Wang, J.-X Yin, P. Dai and P. Bourges, Search for orbital magnetism in the kagome superconductor CsV<sub>3</sub>Sb<sub>5</sub> using neutron diffraction, *Phys. Rev. B*, 110:195109, Nov 2024.
12. C.-Z. Chang, J. Zhang, X. Feng, J. Shen, Z. Zhang, M. Guo, K. Li, Y. Ou, P. Wei, L.-L. Wang, Z.-Q. Ji, Y. Feng, S. Ji, X. Chen, J. Jia, X. Dai, Z. Fang, S.-C. Zhang, K. He, Y. Wang, L. Lu, X.-C. Ma, Q.-K. Xue, Experimental observation of the quantum anomalous Hall effect in a magnetic topological insulator. *Science*, 340:167, Dec 2013.
13. M. Serlin, C. L. Tschirhart, H. Polshyn, Y. Zhang, J. Zhu, K. Watanabe, T. Taniguchi, L. Balents, and A. F. Young Intrinsic quantized anomalous Hall effect in a moiré heterostructure *Science*, 367:900, Dec 2019
14. Yu Zhang, Yifei Ni, Hengdi Zhao, Sami Hakani, Feng Ye, Lance DeLong, Itamar Kimchi, and Gang Cao Control of chiral orbital currents in a colossal magnetoresistance material *Nature*, 611:467, Nov 2022.
15. C. Guo, C. Putzke, S. Konyzheva, X. Huang, M. Gutierrez-Amigo, I. Errea, D. Chen, M.G. Vergniory, C. Felser, M.H. Fischer, T. Neupert and P.J. W. Moll Switchable chiral transport in charge-ordered kagome metal CsV<sub>3</sub>Sb<sub>5</sub> *Nature*, 611:461, Oct 2022.
16. B. Keimer, S A. Kivelson, M. R. Norman, S. Uchida and J. Zaanen, From quantum

22 D. Bounoua, W. Liège, Y. Sidis & Ph. Bourges

- matter to high-temperature superconductivity in copper oxides *Nature*, 518:179, Feb 2015.
17. M. R. Norman, H. Ding, M. Randeria, J. C. Campuzano, T. Yokoya, T. Takeuchi, T. Takahashi, T. Mochiku, K. Kadowaki, P. Guptasarma and D. G. Hinks, Destruction of the Fermi surface in underdoped high- $T_c$  superconductors. *Nature*, 392:157, Mar 1998.
  18. B. Leridon, P. Monod, D. Colson, and A. Forget, Thermodynamic signature of a phase transition in the pseudogap phase of  $\text{YBa}_2\text{Cu}_3\text{O}_x$  high- $T_C$  superconductor, *Europhys. Lett.*, 87:17011, Jul. 2009.
  19. A. Shekhter, B. J. Ramshaw, R. Liang, W.N. Hardy, D.A. Bonn, F. F. Balakirev, R. D. McDonald, J. B. Betts, S. C. Riggs, and A. Migliori, Bounding the pseudogap with a line of phase transitions in  $\text{YBa}_2\text{Cu}_3\text{O}_{6+x}$  *Nature*, 498:75, Jun 2013.
  20. Y. Sato, S. Kasahara, H. Murayama, Y. Kasahara, E.-G. Moon, T. Nishizaki, T. Loew, J. Porras, B. Keimer, T. Shibauchi and Y. Matsuda, Thermodynamic evidence for a nematic phase transition at the onset of the pseudogap in  $\text{YBa}_2\text{Cu}_3\text{O}_y$  *Nat. Phys.*, 13:1074, Nov 2017.
  21. H. Murayama, Y. Sato, R. Kurihara, S. Kasahara, Y. Mizukami, Y. Kasahara, H. Uchiyama, A. Yamamoto, E.-G. Moon, J. Cai, J. Freyermuth, M. Greven, T. Shibauchi and Y. Matsuda, Diagonal nematicity in the pseudogap phase of  $\text{HgBa}_2\text{CuO}_{4+\delta}$  *Nat. Comm.*, 10:3282, Jul 2019.
  22. L. Zhao, C. A. Belvin, R. Liang, D. A. Bonn, W. N. Hardy, W. N. N. P. Armitage, D. Hsieh, A global inversion-symmetry-broken phase inside the pseudogap region of  $\text{YBa}_2\text{Cu}_3\text{O}_y$  *Nat. Physics*, 13:250, Mar 2017.
  23. J. Xia, E. Schemm, G. Deutscher, S. A. Kivelson, D. A. Bonn, W. N. Hardy, R. Liang, W. Siemons, G. Koster, M. M. Fejer and A. Kapitulnik, Polar Kerr-Effect Measurements of the High-Temperature  $\text{YBa}_2\text{Cu}_3\text{O}_{6+x}$  Superconductor: Evidence for Broken Symmetry near the Pseudogap Temperature *Phys. Rev. Lett.*, 100:127002, Mar 2008.
  24. J. Zhang, Z. Zhaofeng, C. Tan, K. Huang, O. O. Bernal, P.-C. Ho, G. D. Morris, A. D. Hillier, Adrian, P. K. Biswas, S. P. Cottrell, H. Xiang, X. Yao, D. E. MacLaughlin and L. Shu, Discovery of slow magnetic fluctuations and critical slowing down in the pseudogap phase of  $\text{YBa}_2\text{Cu}_3\text{O}_y$ , *Science Advances*, 4:eaao5235, Jan 2018.
  25. Zhu, Z. H. and Zhang, J. and Ding, Z. F. and Tan, C. and Chen, C. S. and Wu, Q. and Yang, Y. X. and Bernal, O. O. and Ho, P.-C. and Morris, G. D. and Koda, A. and Hillier, A. D. and Cottrell, S. P. and Baker, P. J. and Biswas, P. K. and Qian, J. and Yao, X. and MacLaughlin, D. E. and Shu, L. Muon spin relaxation and fluctuating magnetism in the pseudogap phase of  $\text{YBa}_2\text{Cu}_3\text{O}_y$  *Phys. Rev. B*, 103:134426, Apr 2021.
  26. B. Fauqué, Y. Sidis, V. Hinkov, S. Pailhès, S. C.T. Lin, X. Chaud, and P. Bourges, Magnetic Order in the Pseudogap Phase of High- $T_C$  Superconductors *Phys. Rev. Lett.*, 96:197001, May 2006.
  27. H. A. Mook, Y. Sidis, B. Fauqué, V. Balédent, and P. Bourges, Observation of magnetic order in a superconducting  $\text{YBa}_2\text{Cu}_3\text{O}_{6.6}$  single crystal using polarized neutron scattering *Phys. Rev. B*, 78:020506, Jul 2008.
  28. Y. Li, V. Balédent, N. Barisic, Y. Cho, B. Fauqué, Y. Sidis, G. Yu, X. Zhao, P. Bourges, and M. Greven, Unusual magnetic order in the pseudogap region of the superconductor  $\text{HgBa}_2\text{CuO}_{4+\delta}$ , *Nature*, 455:372, Sep 2008.
  29. S. De Almeida-Didry, Y. Sidis, V. Balédent, F. Giovannelli, I. Monot-Laffez and P. Bourges, Evidence for intra-unit-cell magnetic order in  $\text{Bi}_2\text{Sr}_2\text{CaCu}_2\text{O}_{8+\delta}$  *Phys. Rev. B*, 86:020504, Jul 2012.
  30. V. Balédent, B. Fauqué, Y. Sidis, N. B. Christensen, S. Pailhès, K. Conder, E. Pomjakushina, J. Mesot, and P. Bourges, Two-dimensional orbital-like magnetic order in the hightemperature  $\text{La}_{2-x}\text{Sr}_x\text{CuO}_4$  superconductor. *Phys. Rev. Lett.* 105:027004, Jul

- 2010.
31. K. Fujita, C. K. and Kim, I. Lee, J. Lee, M. H. Hamidian, I. A. Firmo, S. Mukhopadhyay, H. Eisaki, S. Uchida, M. J. Lawler, E.-A. Kim, and J. C. Davis, Simultaneous Transitions in Cuprate Momentum-Space Topology and Electronic Symmetry Breaking, *Science*, 344:612, May 2014.
  32. T. Ito, K. Takenaka, and S. Uchida, Systematic deviation from T-linear behavior in the in-plane resistivity of  $\text{YBa}_2\text{Cu}_3\text{O}_{7-y}$ : Evidence for dominant spin scattering, *Phys. Rev. Lett.*, 70:3995, Jun. 1993.
  33. V. Balédent, D. Haug, Y. Sidis, V. Hinkov, C. T. Lin, and P. Bourges, Evidence for competing magnetic instabilities in underdoped  $\text{YBa}_2\text{Cu}_3\text{O}_{6+x}$ , *Phys. Rev. B*, 83:104504, Mar 2011.
  34. Z. W. Anderson, Y. Tang, V. Nagarajan, M. K. Chan, C. J. Dorow, G. Yu, D. L. Abernathy, A. D. Christianson, L. Mangin-Thro, P. Steffens, T. Sterling, D. Reznik, D. Bounoua, Y. Sidis, P. Bourges, and M. Greven Gapped commensurate antiferromagnetic response in a strongly underdoped model cuprate superconductor *npj Quantum Materials*, 10:93, Aug. 2025.
  35. P. Bourges and Y. Sidis, Novel magnetic order in the pseudogap state of high-Tc copper oxides superconductors *C. R. Physique*, 12:461, Jun-Aug 2011
  36. L. Mangin-Thro, Y. Li, Y. Sidis, and P. Bourges,  $a-b$  Anisotropy of the Intra-Unit-Cell Magnetic Order in  $\text{YBa}_2\text{Cu}_3\text{O}_{6.6}$ , *Phys. Rev. Lett.*, 118:097003, Mar 2017.
  37. L. Mangin-Thro, Y. Sidis, A. Wildes, P. Bourges, Intra-unit-cell magnetic correlations near optimal doping in  $\text{YBa}_2\text{Cu}_3\text{O}_{6.85}$ , *Nature Communications*, 6:7705, Jul 2015.
  38. Y. Sidis, S. Pailhes, B. Keimer, P. Bourges, C. Ulrich and L.P. Regnault, Magnetic resonant excitations in High- $T_C$  superconductors *Phys. Stat. Sol.(b)*, 241:1204, Apr 2004.
  39. K. Yamada, C. H. Lee, K. Kurahashi, J. Wada, S. Wakimoto, S. Ueki, H. Kimura, Y. Endoh, S. Hosoya, G. Shirane, R. J. Birgeneau, M. Greven, M. A. Kastner and Y. J. Kim, Doping dependence of the spatially modulated dynamical spin correlations and the superconducting-transition temperature in  $\text{La}_{2-x}\text{Sr}_x\text{CuO}_4$  *Phys. Rev. B*, 57:6165, Mar. 1998.
  40. J. M. Tranquada, Neutron Scattering Studies of Antiferromagnetic Correlations in Cuprates in *Handbook of High-Temperature Superconductivity*, 257–298 (Springer, New York, 2007).
  41. P. Bourges, H. Casalta, A. S. Ivanov, and D. Petitgrand, Superexchange Coupling and Spin Susceptibility Spectral Weight in Undoped Monolayer Cuprates *Phys. Rev. Lett.*, 79:4906, Jul.1997.
  42. M.K. Chan, C.J. Dorow, L. Mangin-Thro, Y. Tang, Y. Ge, M.J. Veit, G. Yu, X. Zhao, A.D. Christianson, J.T. Park, Y. Sidis, P. Steffens, D.L. Abernathy, P. Bourges and M. Greven, Commensurate antiferromagnetic excitations as a signature of the pseudogap in the tetragonal high-Tc cuprate  $\text{HgBa}_2\text{CuO}_{4+\delta}$  *Nature Comm.*, 7:10819, Mar 2016.
  43. C. M. Varma, Pseudogap and Fermi arcs in underdoped cuprates, *Phys. Rev. B*, 99:224516, Jun 2019.
  44. S. Lim, C. M. Varma, H. Eisaki, H. and A. Kapitulnik, Observation of broken inversion and chiral symmetries in the pseudogap phase in single- and double- layer bismuth-based cuprates. *Phys. Rev. B*, 105:155103, Apr. 2022.
  45. L. P. Regnault, P. Bourges, and P. Burlet, Phase Diagrams and Spin Correlations in  $\text{YBa}_2\text{Cu}_3\text{O}_{6+x}$ , in *Neutron Scattering in Layered Copper-Oxide Superconductors (ed. Furrer, A.)*, 85–134 (Springer, 1998).
  46. G. L. Squires, Introduction to the Theory of Thermal Neutron Scattering, *Cambridge University Press*, 1978;

24 D. Bounoua, W. Liège, Y. Sidis & Ph. Bourges

47. Y. Sidis, B. Fauque, V. Aji, and P. Bourges, Search for the existence of circulating currents in high-Tc superconductors using the polarized neutron scattering technique *Physica B*, 397:1, Jul 2007.
48. T. C. Hsu, J. B. Marston, and I. Affleck Two observable features of the staggered-flux phase at nonzero doping *Phys. Rev. B*, 43:2866, Feb. 1991.
49. S. Chakravarty, H.Y. Kee, and C. Nayak Neutron scattering signature of d-density wave order in the cuprates *Int. J. Mod. Phys.*, 5:2901, Jun 2001.
50. Y. Tang, L. Mangin-Thro, A. Wildes, M. K. Chan, C. J. Dorow, J. Jeong, Y. Sidis, M. Greven, and P. Bourges Orientation of the intra-unit-cell magnetic moment in the high-Tc superconductor  $\text{HgBa}_2\text{CuO}_{4+\delta}$  *Phys. Rev. B*, 98:214418, Dec 2018.
51. B. J. Kim, H. Ohsumi, T. Komesu, S. Sakai, T. Morita, H. Takagi, and T. Arima Phase-sensitive observation of a spin-orbital Mott state in  $\text{Sr}_2\text{IrO}_4$  *Science* 323:1329, Mar 2009.
52. Y. K. Kim, N. H. Sung, J. D. Denlinger and B. J. Kim, Nature Physics 12, 37 (2016). Observation of a d-wave gap in electron-doped  $\text{Sr}_2\text{IrO}_4$  *Nat. Phys.* 12:37, Jan. 2016.
53. L. Zhao, D. H. Torchinsky, H. Chu, V. Ivanov, R. Lifshitz, R. Flint, T. Qi, G. Cao, and D. Hsieh Evidence of an odd-parity hidden order in a spin-orbit coupled correlated iridate. *Nat. Phys.* 12:32, Jan 2016.
54. S. Chatterjee and S. Sachdev, Insulators and metals with topological order and discrete symmetry breaking *Phys. Rev. B* 95:205133, May 2017.
55. S. Chatterjee, S. Sachdev and M.S. Scheurer, Intertwining Topological Order and Broken Symmetry in a Theory of Fluctuating Spin-Density Waves *Phys. Rev. Lett.*, 119:227002, Nov 2017.
56. X. Feng, K. Jiang, Z. Wang, and J. Hu, Chiral flux phase in the Kagome superconductor  $\text{AV}_3\text{Sb}_5$ , *Sci. Bull.*, 66:1384, Jul 2021.
57. Y.-P. Lin and R. M. Nandkishore, Complex charge density waves at Van Hove singularity on hexagonal lattices: Haldanemodel phase diagram and potential realization in the kagome metals  $\text{AV}_3\text{Sb}_5$  (A=K, Rb, Cs), *Phys. Rev. B*, 104:045122, Jul 2021.
58. S. Zhou and Z. Wang, Chern fermi pocket, topological pair density wave, and charge-4e and charge-6e superconductivity in kagome superconductors, *Nat. Commun.*, 13:7288, Nov 2022.
59. H. Li, T. T. Zhang, T. Yilmaz, Y. Y. Pai, C. E. Marvinney, A. Said, Q.W. Yin, C. S. Gong, Z. J. Tu, E. Vescovo, C. S. Nelson, R. G. Moore, S. Murakami, H. C. Lei, H. N. Lee, B. J. Lawrie, and H. Miao, Observation of unconventional charge density wave without acoustic phonon anomaly in kagome superconductors  $\text{AV}_3\text{Sb}_5$  (A = Rb, Cs), *Phys. Rev. X*, 11:031050, Sep 2021.
60. F. H. Yu, T. Wu, Z. Y. Wang, B. Lei, W. Z. Zhuo, J. J. Ying, and X. H. Chen Concurrence of anomalous Hall effect and charge density wave in a superconducting topological kagome metal *Phys. Rev. B*, 104:L041103 Jul 2021.
61. F. D. M. Haldane, Model for a quantum Hall effect without Landau levels: Condensed-matter realization of the “parity anomaly”, *Phys. Rev. Lett.*, 61:2015, Oct 1988.
62. C. Mielke, III, D. Das, J.-X. Yin, H. Liu, R. Gupta, Y.-X. Jiang, M. Medarde, X.Wu, H. C. Lei, J. Chang, P. Dai, Q. Si, H. Miao, R. Thomale, T. Neupert, Y. Shi, R. Khasanov, M. Z. Hasan, H. Luetkens, and Z. Guguchia, Time-reversal symmetry-breaking charge order in a kagome superconductor, *Nature*, 602:245, Feb 2022.
63. H. Deng, G. Liu, Z. Guguchia, T. Yang, J. Liu, Z. Wang, Y. Xie, S. Shao, H. Ma, W. Liège, F. Bourdarot, X.-Y. Yan, H. Qin, C. Mielke III, R. Khasanov, H. Luetkens, X. Wu, G. Chang, J. Liu, M.H. Christensen, A. Kreisel, B. M. Andersen, W. Huang, Y. Zhao, P. Bourges, Y. Yao, P.-C. Dai and J.-X. Yin Evidence for time-reversal symmetry-breaking kagome superconductivity *Nat. Mat.*, 23:1639, Aug 2024.

64. J. Kang, and Z. Tesanovic, Theory of the valley-density wave and hidden order in iron pnictides *Phys. Rev. B*, 83:020505, Jan 2011.
65. W. Klug, J. Kang, R.M. Fernandes, and J. Schmalian, Orbital loop currents in iron-based superconductors *Phys. Rev. B*, 97:155130, Apr 2018.
66. S. W. Lovesey, T. Chatterji, A. Stunault, D. D. Khalyavin, and G. van der Laan, Direct observation of anapoles by neutron diffraction *Phys. Rev. Lett.*, 122:047203, Feb. 2019.
67. S. W. Lovesey, J. Fernandez-Rodriguez, J. A. Blanco, D. S. Sivia, K. S. Knight, and L. Paolasini, Vanadium magnetoelectric multipoles in  $V_2O_3$  *Phys. Rev. B*, 75:014409 Jan 2007.
68. S. Bhowal S, N. Spaldin, Ferroically Ordered Magnetic Octupoles in  $d$ -Wave Altermagnets *Phys. Rev. X*, 14:011019, Feb. 2024.
69. P. McClarty, J. Rau Landau Theory of Altermagnetism *Phys. Rev. Lett.*, 132:176702, Apr 2024.
70. V. E. Dmitrienko and V. A. Chizhikov, Hidden order in  $URu_2Si_2$ : Symmetry-induced antitoroidal vortices *Phys. Rev. B*, 98:165118, Oct. 2018.
71. C. Silva de Farias, M.-A. Méasson, A. Ferraz, and S. Burdin, Effective model for the  $A_{2g}$  Raman signal in  $URu_2Si_2$  *Phys. Rev. B*, 101:205114, May 2020.
72. D. F. Agterberg, D. S. Melchert, M. K. Kashyap, Emergent loop current order from pair density wave superconductivity *Phys. Rev. B* 91:054502, Feb 2015.
73. Y. Liu, and V. Aji, Bond ordering in flux phases of interacting spinless fermions on the square lattice *Phys. Rev. B*, 113:045140, Jan 2026.